Morphological and Crystallographic Characterization of Nanoparticles by Granulometry Image Analysis and Rietveld Refinement Methods

Ganjkhanlou, Yadolah•
Department of Physical Chemistry, Faculty of Chemical Technology, University of Pardubice, Studentská 573, CZ-532 10 Pardubice, Czech Republic

Bayandori Moghaddam, Abdolmajid*+
School of Engineering Science, College of Engineering, University of Tehran, P.O. Box 11155-4563 Tehran, I.R. IRAN

ABSTRACT: *The particle size distribution of the resultant cobalt ferrite samples was determined from Scanning Electron Microscopy (SEM) images using the granulometry image analysis method. The results showed the nanosized particles of the samples. The X-Ray Diffraction (XRD) patterns of samples were also analyzed by Rietveld refinement method. The results indicated that the precipitated sample at 95 °C had cubic cobalt ferrite structure with F3dm:3 space group and high crystallinity. The lattice parameters, microstrain and crystallite size of samples were also calculated from the XRD pattern. With increasing the precipitation temperature, the crystallite and particle sizes were increased while the lattice parameter and microstrain were decreased. Regarding the results, it can be concluded that the lattice parrameter of cobalt ferrite has a diverse relationship with crystallite size.*

KEYWORDS: *Local thresholding algorithm; X-ray diffraction; Image processing; Particle size distribution.*

INTRODUCTION

The physical and chemical properties of materials are depended to the particle size especially in nanometer scale due to their large surface-to-volume ratio [1-7]. For this reason, nanomaterials have received considerable attention in recent years [8-12]. Their unique properties have presented novel applications and have been widely studied [13-15]. Nanomaterials with magnetic properties have been using in technological applications and fundamental studies [16,17]. Magnetic nanoparticles and their suspensions have been used as optical devices [18], sensors [19], magnetic resonance imaging, [20], magnetically guided drug delivery and cancer therapy [21,22]. Cobalt ferrite is one of the promising compounds, applied as magnetic materials in various

* *To whom correspondence should be addressed.*
+ *E-mail: bayandori@ut.ac.ir*
• *Other Address: Materials and Energy Research Center, P.O. Box 14155-4777, Tehran, I.R. IRAN*
1021-9986/2019/1/11-16 6/$/5.06

functions. It also shows strong anisotropy, high microwave magnetic loss, and moderate saturation magnetization at room temperature [23]. Various electrochemical, sol-gel, mechanical alloying, micro-emulsion, physical vapor deposition, and laser deposition methods were presented for preparation of cobalt ferrite nanoparticles and films [23-28]. But, the majorities of these methods require high treatment or post annealing temperature in order to enhance the crystallinity and magnetic properties of cobalt ferrite.

The facility of data gathering in the X-Ray Diffractometry (XRD) makes it the prominent characterization method in material science. Usually the XRD pattern was utilized for phase determination and crystallite size estimation with scherrer's relation. However, many sophisticated methods such as Rietveld refinement can be applied for accurate determination of phase structure and structural parameters such as lattice parameter, bond length, and cell volume as well as microstructural parameters (texture, crystallite size, micro strain) [29-32].

In this work, we attempt to utilize the granulometry image analysis and the Rietveld refinement method to elaborate characterization of synthesized nanoparticles beside common techniques. Cobalt ferrite nanoparticles were prepared with appropriate crystallinity without the requirement of post annealing.

EXPERIMENTAL SECTION

Chemical reagents

The 120 mL aqueous solution containing 80 mM $FeCl_3.6H_2O$ and 40 mM $Co(CH_3COO)_2.4H_2O$ was added very slowly into the 120 mL of 640 mM NaOH under stirring. The temperature of the reaction beaker maintained at about 55 ºC. The solution of Fe^{3+} and Co^{2+} cations were added to the beaker. Afterward, the precipitates (sample A) were dried in the air [8]. This process was repeated at 95 ºC for obtaining the sample B. The used salts were reagent grade materials from Merck. All solutions were prepared with deionized water.

Characterization of samples

Scanning Electron Microscopy (SEM) investigations were carried out using a Cambridge electron microscope, model Steroscan 360. The SEM images of samples were assessed using the granulometry image analysis method in order to determine mean particle size and its distribution. Fig. 1 shows the processes used for this purpose.

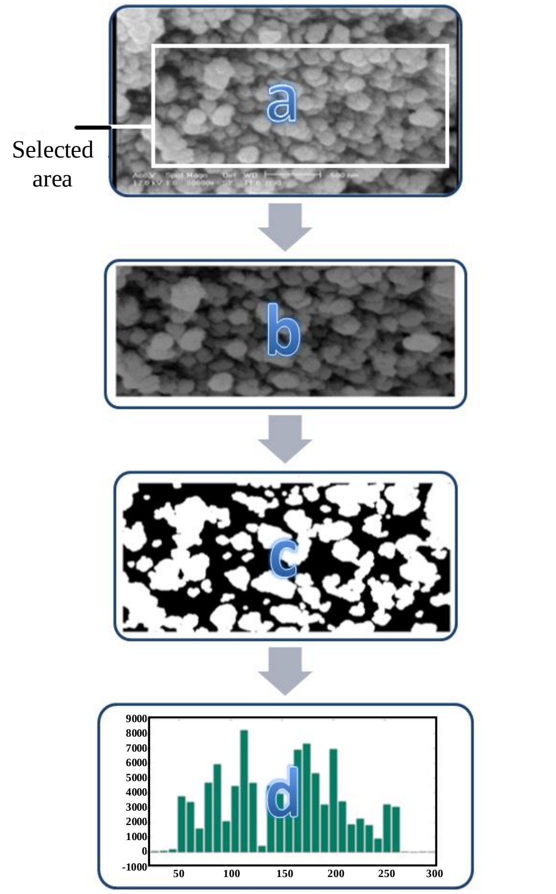

Fig. 1: Procedure of granulometry (a) selected initial image (b) Smoothed version of a selected area on initial image (c) The binary image of smoothed image using local thresholding (d) histogram of particle diameter distribution produced by morphological techniques.

In accordance with parts (a) and (b) of this figure, the erosion and dilation of the SEM image of sample B were smoothed by image histogram adjustment. In part (c) of Fig. 1, the enhanced image was converted to the binary image by a local thresholding algorithm. Eventually, the particle size distribution can be computed by applying for the morphological opening of increasing size. For each opening, the sum of all the pixel value in it was computed. This sum is well known as surface area of image [33]. The surface area of image can be plotted against radii of disk shaped opening. The surface area will be reduced between the successful openings. Regarding these statements, the negative value of surface area differential versus diameter of disc shaped opening is equal to the particle size distribution (part (d) of Fig. 1).

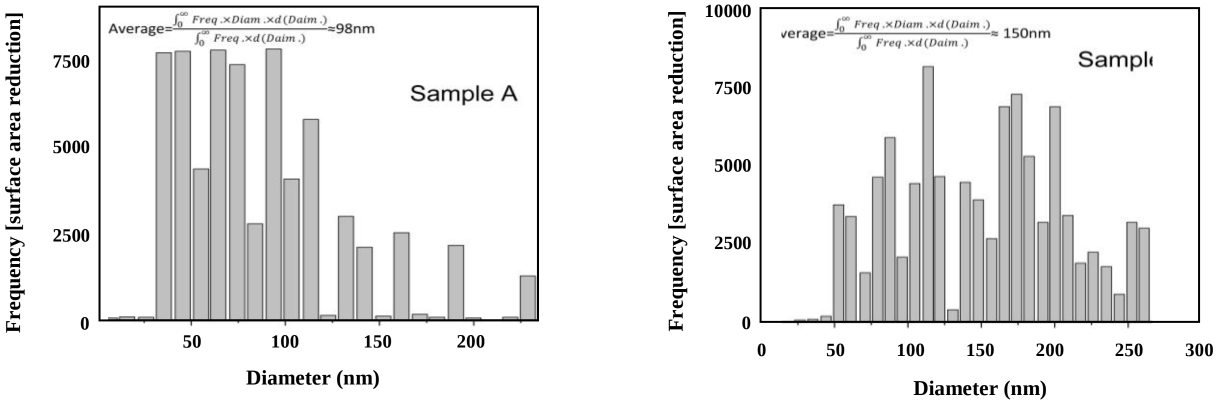

Fig. 2: Particle size distribution of samples A and B calculated by image analysis granulometry method.

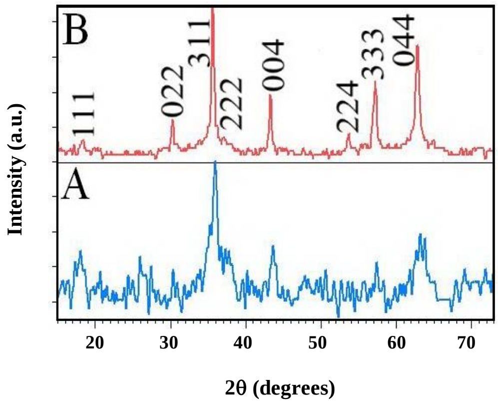

Fig. 3: XRD patterns of as prepared samples.

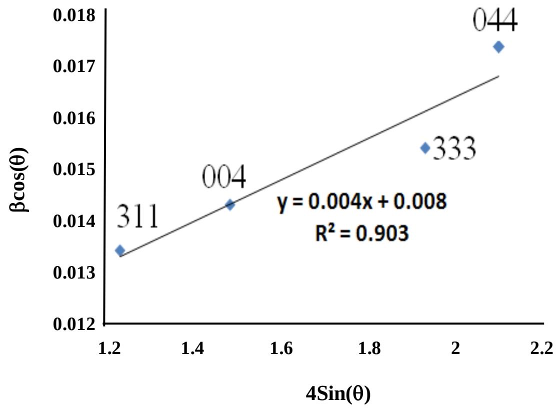

Fig. 4: Williamson-Hall plot of sample A.

The microstructure and structure of samples were also determined from X-Ray Diffraction analysis (XRD, Philips X'Pert diffractometer) by Rietveld refinement method. Rietveld refinement [29] was performed using MAUD Software [30,31]. The software calibrated by Si standard sample (NBS 640) free from the effect of reduced crystallite size and lattice defects.

RESULTS AND DISCUSSION

Parts (a) and (b) of Fig. 2 depict the particle size distribution of sample A and B calculated by image analysis granulometry. It can be seen that with increasing the precipitation temperature, the particle sizes were enhanced.

Fig. 3 illustrates the recorded XRD pattern of Samples A and B. Comparing the XRD pattern broadening and counts, it can be comprehended that Sample A with lower precipitation temperature, has lower crystallinity in comparison with Sample B. Also, it is appreciated that both samples have a cubic inverse spinel structure of $CoFe_2O_4$ with Fd-3m:1 space group. As can be seen from Fig. 3, Sample A has a noisy XRD pattern because of the low crystallinity. Therefore, for this sample, the Rietveld refinement with reliable result could not be performed. For Sample A, the lattice parameter computed by Bragg's law considering the main diffraction line position. The microstrain and crystallite size of same sample were calculated by Williamson-Hall plot [34] using the (311), (004), (333) and (044) lines. Fig. 4 depicts this plot for Sample A and Equation (1) shows the method of the microstrain and crystallite size determination.

$$\beta\cos(\theta) = \lambda/D + 4\varepsilon \sin(\theta) \quad (1)$$

In equation (1), β denotes the XRD lines broadening that are free from instrument broadening, λ=Wave length of X-ray tube (Cu kα), D=crystallite size, ε=microstrain, and θ denotes the angle of diffraction.

Table 1: The cryastallographic and microstructural parameters of as prepared samples.

Sample	a (nm)	D (nm)	ε	R%	P (nm)
A	0.843	37.6	0.005	----	98.450
B	0.839	97.59	0.0021	9.45	150.03

a=lattice parameter, D=crystallite size, ε=microstrain, R=agreement factor of refinement, P=mean value of particle size calculated from SEM images

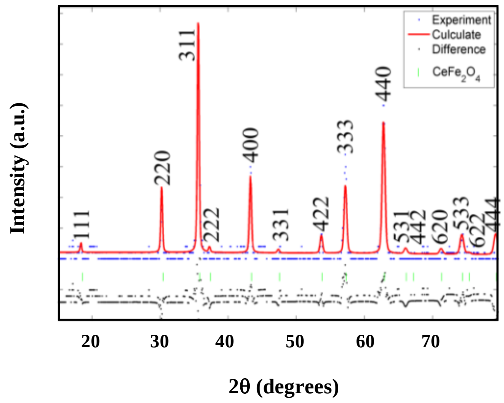

Fig. 5: Recorded XRD pattern (dot) and Rietveld calculated pattern of Sample B. the diffrences of these two patterns is also shown in the figure. The bars illustrate the possition of the cobalte ferrite diffraction lines.

Fig. 5 illustrates the recorded XRD pattern of Sample B (dots) besides Rietveld calculated XRD pattern (solid line) and the differences of the calculated and experimental pattern. Results of these calculations were listed in Table 1. The agreement factor of refinement was shown for Sample B in this table which is smaller than 10% indicating the riability of refined parameters. From Table 1, both samples had nanosized crystallites and crystallite size and particle size was enhanced with increasing the precipitation temperature from 55 to 95 ºC. While the lattice parameter and microstrain were decreased. Results also showed that the lattice parrameter of cobalt ferrite has a diverse relationship with crystallite size. In nanomaterials, the surface area is higher than the balk materials. Therefore, the number of surface atoms is higher than bulk materials and the average strength of bonds are lower. Consequently, the lattice parameter in nano materials will expand.

CONCLUSIONS

Cobalt ferrite nanoparticles were synthesized at 55 ºC and 95 ºC. SEM image and the XRD pattern of samples were analyzed by the granulometry image analysis and Rietveld refinement method, respectively. The reported results indicated that the prepared sample at 95 ºC has high crystallinity with F3dm:3 space group. With increasing the temperature, crystallite and particle sizes were enhanced while the lattice parameter and microstrain were decreased. Also, the lattice parrameter of cobalt ferrite has diverse relationship with crystallite size.

Acknowledgments

The authors would like to thank the Research Affairs of the University of Tehran.

Received : Feb. 24, 2017 ; Accepted : Dec. 18, 2017

REFERENCES

[1] Cao X., Gu L., Spindly Cobalt Ferrite Nanocrystals: Preparation, Characterization and Magnetic Properties, *Nanotechnology*, **16**: 180-185 (2005).

[2] Dabaghi H.H., Ganjkhanlou Y., Kazemzad M., Moghaddam A.B., Relation between Conductance, Photoluminescence Bands and Structure of ITO Nanoparticles Prepared by Various Chemical Methods, *Micro Nano Lett.*, **6**: 429-433 (2011).

[3] Bagheri M., Karimkoshteh M., One-Pot Reduction of Aromatic Carboxylic Acid to Alcohol by SiO_2@$FeSO_4$ Nanocomposite at Solvent-Free Condition, *Iran. J. Chem. Chem. Eng. (IJCCE)*, **36**: 37-43 (2017).

[4] Khashi M., Allameh S., Beyramabadi S.A., Morsali A., Dastmalchian E., Gharib A., $BiFeO_3$ Magnetic Nanoparticles: A Novel, Efficient and Reusable Magnetic Catalyst for the Synthesis of Polyhydroquinoline Derivatives, *Iran. J. Chem. Chem. Eng. (IJCCE)*, **36**: 45-52 (2017).

[5] Moghaddam A.B., Electrodeposited Nanoscale Zinc Oxide Particles: Facilitating the Electron Transfer of Immobilised Protein and Biosensing, *Micro Nano Lett.*, **12**: 425-429 (2017).

[6] Razeghizadeh A.R., Zalaghi L., Kazeminezhad I., Rafee V., Growth and Optical Properties Investigation of Pure and Al-Doped SnO_2 Nanostructures by Sol-Gel Method, *Iran. J. Chem. Chem. Eng. (IJCCE)*, **36**: 1-5 (2017).

[7] Hamedi S., Shojaosadati S.A., Shokrollahzadeh S., Hashemi-Najaf Abadi S., Controlled Biosynthesis of Silver Nanoparticles Using Culture Supernatant of Filamentous Fungus, *Iran. J. Chem. Chem. Eng. (IJCCE)*, **36**: 33-42 (2017).

[8] Moghaddam A.B., Hosseini S., Badraghi J., Banaei A., Hybrid Nanocomposite Based on $CoFe_2O_4$ Magnetic Nanoparticles and Polyaniline, *Iran. J. Chem. Chem. Eng. (IJCCE)*, **29**: 173-179 (2010).

[9] Mohammadi A., Ganjkhanlou Y., Kazemzad M., Moghaddam A.B., Hessari F.A., Dinarvand R., Effect of Strontium Doping on Nanostructure and Chromaticity of Y_2O_3:Eu Compounds, *Int. J. Modern Phys. B*, **25**: 2949-2956 (2011).

[10] Mohammadi A., Ganjkhanlou Y., Moghaddam A.B., Kazemzad M., Hessari F.Al., Dinarvand R., Synthesis of Nanocrystalline Y_2O_3:Eu Phosphor Through Different Chemical Methods: Studies on the Chromaticity Dependence and Phase Conversion, *Micro Nano Lett.*, **7**: 515-518 (2012).

[11] Nabid M.R., Shamsianpour M., Sedghi R., Moghaddam A.B., Enzyme-Catalyzed Synthesis of Conducting Polyaniline Nanocomposites with Pure and Functionalized Carbon Nanotubes, *Chem. Eng. Technol.*, **35**: 1707–1712 (2012).

[12] Khajeamiri A.R., Kobarfard F., Moghaddam A.B., Application of Polyaniline and Polyaniline/Multiwalled Carbon Nanotubes-Coated Fibers for Analysis of Ecstasy, *Chem. Eng. Technol.*, **35**: 1515-1519 (2012).

[13] Burda C., Chen X.B., Narayanan R., El-Sayed M.A., Chemistry and Properties of Nanocrystals of Different Shapes, *Chem. Rev.*, **105**: 1025-1102 (2005).

[14] Ganjkhanlou Y., Hosseinnia A., Kazemzad M., Moghaddam A.B., Khanlarkhani A., Y_2O_3: Eu, Zn Nanocrystals as a Fluorescent Probe for the Detection of Biotin, *Microchim. Acta*, **177**: 473-478 (2012).

[15] Mohammadi A., Moghaddam A.B., Direct Electrochemistry and Electrocatalysis of Immobilised Cytochrome c on Electrodeposited Nanoparticles for the Reduction of oxygen, *Micro Nano Lett.*, **7**: 951-954 (2012).

[16] Moghaddam A.B., Esmaieli M., Khodadadi A.A., Ganjkhanlou Y., Asheghali D., Direct Electron Transfer and Biocatalytic Activity of Iron Storage Protein Molecules Immobilized on Electrodeposited Cobalt Oxide Nanoparticles, *Microchim. Acta*, **173**: 317-322 (2011).

[17] Pnakhurst Q.A., Connolly J., Jones S.K., Cobson J., Applications of Magnetic Nanoparticles in Biomedicine, *J. Phys. D*, **36**: R167 (2003).

[18] Fontijn W.F.J., Van der Zaag P.J., Devillers M.A.C., Brabers V.A.M., Metselaar R., Optical and Magneto-Optical Polar Kerr Spectra of Fe_3O_4 and Mg^{2+} or Al^{3+} Substituted Fe_3O_4, *Phys. Rev. B*, **56**: 5432-5442 (1997).

[19] Mohammadi A., Moghaddam A.B., Badraghi J., Direct Electron Transfer of Ferritin on Electrodeposited Nickel Oxide Cubic Nanoparticles, *Anal. Methods*, **4**: 1024-1028 (2012).

[20] Bergemann C., Muller-Schulte D., Oster J., Brassard L., Lubbe A.S. J., Magnetic Ion-Exchange Nano- and Microparticles for Medical, Biochemical and Molecular Biological Applications, *J. Magn. Magn. Mater.*, **194**: 45-52 (1999).

[21] Tartaj P., Morales P.M., Veintemillas-Verdaguer S., Gonzalez-Carreno T., Serna C.J., The Preparation of Magnetic Nanoparticles for Applications in Biomedicine, *J. Phys. D*, **36**: 182-197 (2003).

[22] Kaufner L., Cartier R., Wustneck R., Fichtner I., Pietschmann S., Bruhn H., Schutt D., Thunemann A.F., Pison U., One-Pot Reaction to Synthesize Biocompatible Magnetite Nanoparticles, *Nanotechnology*, **18**: 115710 (2007).

[23] Yuan J.J., Zhao Q., Xu Y.S., Liu Z.G., Du X.B., Wen G.H., Synthesis and Magnetic Properties of Spinel $CoFe_2O_4$ Nanowire Arrays, *J. Magn. Magn. Mater.*, **321**: 2795-2798 (2009).

[24] Liu C., Zou B., Rondinone A.J., Zhang Z.J., X-ray Diffraction Pattern of as-Prepared FePt Nanoparticles, *J. Am. Chem. Soc.*, **122**: 6263-6267 (2000).

[25] Sivakumar N., Narayanasamy A., Shinoda K., Chinnasamy C.N., Jeyadevan B., Greneche J.-M., Electrical and Magnetic Properties of Chemically Derived Nanocrystalline Cobalt Ferrite, *J. Appl. Phys.*, **102**: 013916-013916 (2007).

[26] Zhang L., Li Z., Study of Nanocrystalline FeSi Alloys Prepared by Mechanical Alloying, *J. Alloys Comp.*, **469**: 422-426 (2009).

[27] Bao N., Shen L., Wang Y., Padhan P., Gupta A., Organic Molecule-Assisted Hydrothermal Self-Assembly of Size-Controlled Tubular ZnO Nnostructures, *J. Am. Chem. Soc.*, **129**: 12374-12375 (2007).

[28] Ahmed S.R., Ogale S.B., Papaefthymiou G.C., Ramesh R., Kofinas P., Magnetic Properties of $BiFeO_3$-$BaTiO_3$ Solid Solution Nanostructures, *Appl. Phys. Lett.*, **80**: 1616-1618 (2002).

[29] Rietveld H.M., Rietveld Refinement an Industry Standard, *J. Appl. Cryst.*, **2**: 65-71 (1969).

[30] Lutterotti L., Ceccato R., Maschio R.D., Pagani E., Quantitative Analysis of Materials by the Rietveld Method, *Mater. Sci. Forum*, **93**: 278-281 (1998).

[31] Lutterotti L., Gialanella S., X-ray Diffraction Characterization of Heavily Deformed Metallic Specimens, *Acta Mater.*, **46**: 101-108 (1998).

[32] Torkaman N.M., Ganjkhanlou Y., Kazemzad M., Dabaghi H.H., Keyanpour-Rad M., Crystallographic Parameters and Electro-Optical Constants in ITO Thin Films, *Mat. Charact.*, **61**: 362-370 (2010).

[33] Gonzalez R.C., Woods R.E., Eddins S., "Digital Image Processing Using Matlab", Prentice Hall, New Jersey (2004).

[34] Williamson G.K., Hall W.H., X-Ray Line Broadening from Filed Auminium and Wolfram, *Acta Metall.*, **1**: 22-31 (1953).